BALLISTIC PHASE MANAGEMENT FOR CRYOGENIC UPPER STAGES

P. Behruzi, F. de Rose, P. Netzlaf, H. Strauch,
Astrium GmbH, Airbus-Allee 1, 28199 Bremen

Abstract

Ballistic flight phases for cryogenic upper stages impose the need to analyze the sloshing behaviour in the propellant tanks, taking into account the RCS manoeuvres as well as the temperature evolution. A tool was therefore developed which enables a closed loop analysis of the stage behaviour, taking into account the stage controller as well as the fluid dynamics in the tank. In addition a coupling of the propellant thermodynamics in the tank, modelled with the CFD tool FLOW-3D, and the thermodynamics of the stage structure, modelled with the tool ESATAN, was set up. First steps concerning a verification of the tool were conducted. The strong interaction between propellant sloshing in the tanks and the RCS thruster activations show the need to take a coupling between rigid body motion and the fluid dynamics into account.

1. INTRODUCTION

The next generation of cryogenic upper stages is expected to carry out multiple restarts with coasting phases of varying durations with up to 5.5 hours. Applications are for example flights to the International Space Station ISS, terrestrial and extraterrestrial satellite missions with more than one upper stage engine firing. A further operational mode is the GTO+ orbit release, which also requests a second main engine restart close to the apogee of a GTO mission.

In case of a GTO/GTO+ mission two payload release sequences occur. The first payload is released in a "classical" way immediately after the first main engine shut down. At that point in time there will be much propellant left, which is needed for the second re-boost (filling levels in the order of 20 % to 40 %) necessary for a GTO+ orbit. This means that the first payload release phase has to cope with a sloshing mass, which is much higher than in the past, e.g. in case of the Ariane 5 ESC-A upper stage. The sloshing frequencies and the coupling factors are correlated with the sloshing mass. If the payload release accuracy is requested to be high, then the controller bandwidth is large. Coupling with the flexible sloshing mode may then lead to the loss of closed loop stability.

Up to now this never was of much concern for the present Ariane 5 ESC-A upper stage, due to the low remaining tank filling levels. Consequently the controller design seldom took the sloshing frequencies into account and the stability was only checked after the design phase. The higher sloshing mass may now require a design taking the sloshing phenomenon into account right away. In case the design already indicates a certain proximity to the stability boundary, a tool for sloshing simulation is needed, which is not as conservative as the current pendulum or spring/damper models are. Replacing these phenomenological models with a CFD fluid simulation tool like FLOW3D® [3] is the result of this work and a major improvement for future development.

During the A5ME development, which started in 2009, a further problem area manifested itself. The long duration of the ballistic flight between the main engine shut down and engine re-ignition made an estimate of the torques, generated by the propellant during that period, important. These reaction torques of the fluid (in a state of zero g) are disturbance torques, when seen from the controller point of view. They will induce corrective attitude commands, which will increase the propellant consumption needed for attitude stabilization. For this kind of analysis the pendulum or spring/damper models are completely un-useable. Again the need for a coupled simulation with the actual flight algorithm and a CFD fluid simulator manifested itself.

A second issue with respect to cryogenic upper stages is the thermal behavior of the cold propellants during a ballistic phase. The dynamic sloshing behavior of the liquid, e.g. during RCS activations, may quickly change wall temperatures and corresponding evaporation rates. Once surfaces become dry they can also quickly heat up. An accurate prediction of the thermal behavior, in combination with the rigid body motion during the ballistic flight phase, is thus of great interest.

A closed loop simulation tool, called FiPS (Final Phase Simulator), was therefore set up, which is able to model these phenomena without recourse to simple pendulum models. The tool includes a coupling algorithm of the CFD tool FLOW-3D® [3] and the ESATAN software [4]. The software ESATAN is employed for the analysis of thermal conditions within structures.

The following chapters first give an overview on the FiPS tool. Thereafter different verification and application cases are discussed.

2. THEORETICAL BACKGROUND

2.1. Coupling algorithm between the rigid body modelization and the FLOW-3D® model through FiPS

One advantage of the FiPS code is the possibility to have access to output data generated by the software tool calculating the propellant motion (equivalent pendulum / mass spring or CFD code) before passing it to the rigid body algorithm. At Astrium coupling has been realized with the CFD software FLOW-3D® by Flow Science [3]. Using FiPS it is possible to check and if necessary to filter the CFD output data ensuring that no numerical disturbances influence the rigid body motion.

A simplified schematic representation of the interaction between FiPS and FLOW-3D® is shown in Fig. 1. An overall simulation environment structure is also given in Fig. 2.

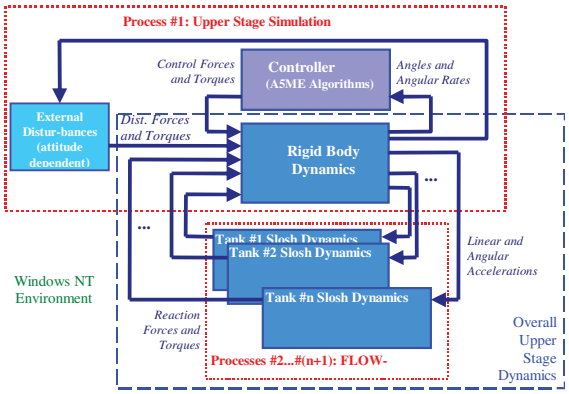

Fig. 1 Simplified representation of the interaction between the rigid body modelization and the FLOW-3D® model through FiPS

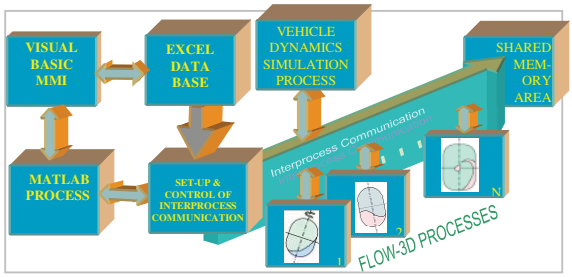

Fig. 2 Overall Simulation Environment structure

The rigid body model exchanges acceleration as well as force and torque data with the fluid dynamic model. Furthermore simplified models, such as spring-mass models, can be coupled to FiPS in the same manner as done with the FLOW-3D® model in the present case. Thus it is possible to compare the simplified models with the CFD computation and by way of modifying the pendulum parameter to adapt them in a more sophisticated way.

As an example Fig. 3 shows the sloshing motion in case of a spin-up maneuver. The picture shows the tank configuration of the Ariane A5ME upper stage.

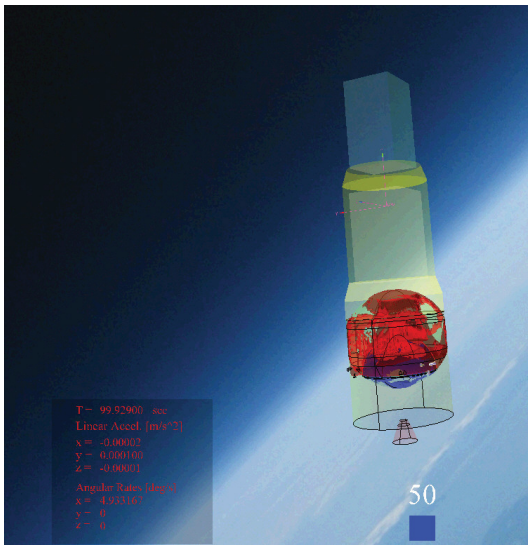

Fig. 3 Propellant sloshing motion inside the LH2 tank (top) and the LOX tank (bottom) in case of spin-up manoeuvre (here Ariane A5ME upper stage)

The picture shows the reorientation of the liquid towards the tank wall when the stage goes into a spin motion (here 5 °/s). As shown in Fig. 3 the propellant motion in the tanks is generally very chaotic making it difficult to understand and verify the liquid motion. Thus a visualization tool has been developed allowing the visual observation of the propellant motion inside the tanks including the motion of the stage and the thrust pulses, see Fig. 4.

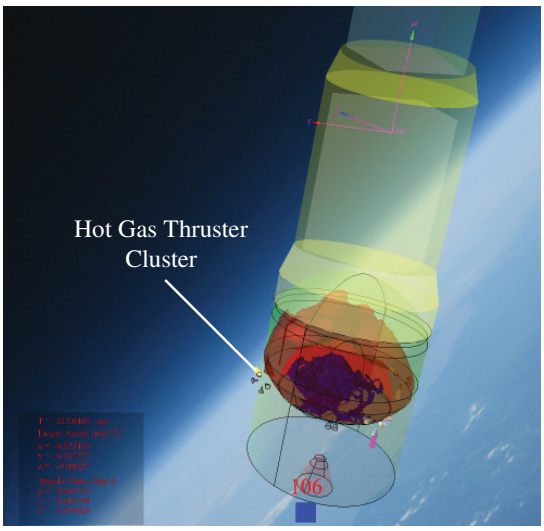

Fig. 4 Propellant sloshing motion inside cryogenic upper stage tanks (here Ariane A5ME upper stage) and corresponding cold gas and hot gas thrust pulse during a re-orientation maneuver.

2.2. FLOW-3D / ESATAN Coupling

In a second step a coupling between the CFD code FLOW-3D and the thermal code ESATAN is included. A single CFD process (FLOW-3D) and an ESATAN process is started for each tank separately. Data are exchanged between the respective processes (see Fig. 5 below).

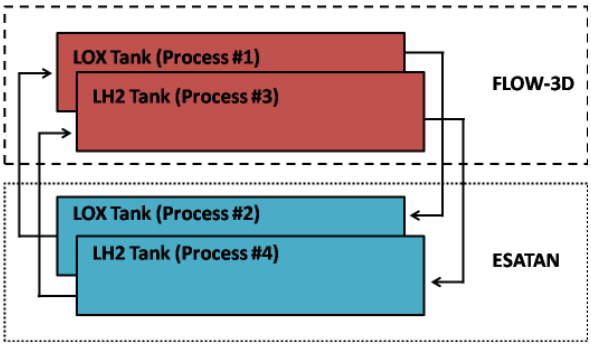

Fig. 5. For each tank a single CFD process (FLOW-3D) and an additional ESATAN process is started. Data are exchanged in between the processes.

A more detailed view of the coupling algorithm is given in Fig. 6.

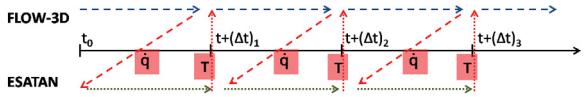

Fig. 6. Data exchange between FLOW-3D and ESATAN

The FLOW-3D process computes its first time step by means of its initial conditions, including the temperatures provided by ESATAN. At the end of the first time step the FLOW-3D process is stopped, the calculated data is written to the respective part of the shared data area and it is kept waiting. Afterwards the next process, that is ESATAN, is initiated. It obtains the length of the first time step as well as the heat fluxes of all the nodes, which have already been calculated by the first process, and conducts the calculation for this time step on its part. This is done for every process, whereas the FLOW-3D processes are always the clocking ones.

The exchange between the two programs is organized such that a dedicated cell is prescribed for every boundary cell in the CFD analysis. Generally this leads to a relatively high resolution of the tank for the ESATAN model. An example concerning the Ariane 5 ESC-A LOX tank is given in Fig. 7. The left picture shows the tank in the CFD analysis (FLOW-3D). The right picture shows the corresponding tank defined for the ESATAN software.

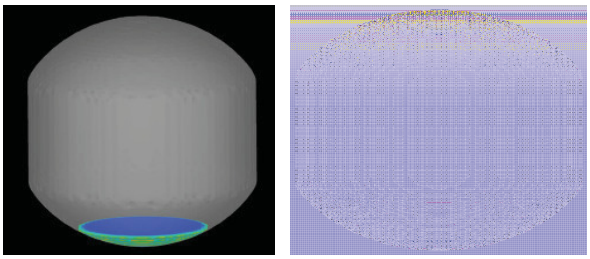

Fig. 7. Ariane 5 ESC-A LOX tank as defined for the CFD model (FLOW-3D, left) and the corresponding ESATAN model (right)

3. VERIFICATION

3.1. Testing of the simulator

For verification of the FiPS simulator it is necessary to define test cases representing relevant flight sequences occurring during a mission. A test of the functionality of the attitude control during powered flight where the main engine is used for generation of the control torques can be simply defined forcing a change of the attitude angle. Currently the attitude control is limited to regulate the attitude angle according the commanded attitude. Guidance allows following a given trajectory which is not yet foreseen.

The simulation of a typical manoeuvre sequence of a ballistic phase can be used to test and validate the simulator part active in a ballistic part of a flight manoeuvre. One candidate for testing the simulator is a spin-up sequence with nutation damping. The test case consists of a manoeuvre sequence containing necessary commands.

Combining both, the powered flight and the ballistic phase, a test case can be defined containing both phases successively. Test and verification is done using such a manoeuvre sequence.

In addition to the mass properties and the parameters for the gimbal and attitude controllers, the commanded angels and the duration time for the manoeuvre are specified.

The simulation results are shown in the following Fig. 8 to Fig. 13. The comparison of the quantities shows clearly the impact of the sloshing on the behaviour of the composite. Comparing the rigid body simulation with the results of the simulations coupled with FLOW-3D and those coupled with a spring damper model, representing the sloshing behaviour, the difference in the impact of the different sloshing sources on the behaviour of the composite is significant for instance in the angular rates profile. As can be seen in Fig. 8 (spin-up, axis ar(1)) the rigid body simulation has a stronger rising edge of the transient phase as the simulations with coupled sloshing. Also the steady state is reached faster. Here the biggest impact of the sloshing mass is found.

During the first 8 seconds only the main thruster is active for attitude control. During this phase the reaction control

thrusters are only used for roll control. In Fig. 9 the Euler Angles, representing the attitude of the vehicle, are shown. Starting from the initial attitude (x=0°, y=0°, z=0°) the attitude changes to commanded attitude (x=0°, y=-5°, z=4°) and is kept until the spin-up manoeuvre starts. After reaching steady state the observer estimates the nutation damping. Thereafter the controller for nutation control is activated and the nutation angles on the transversal axes are limited.

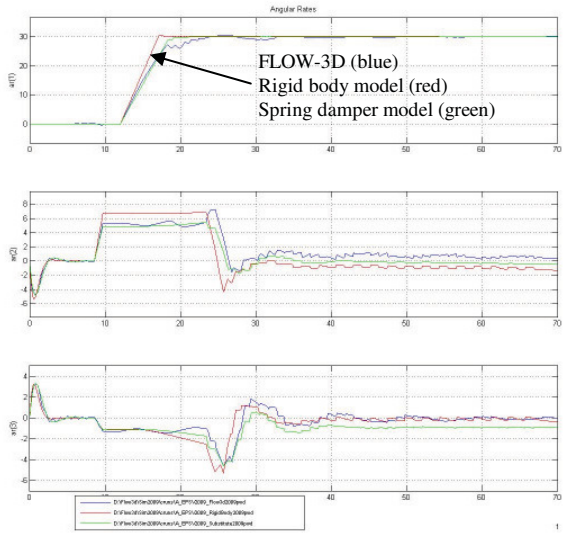

Fig. 8 Comparison of the simulation results (Angular Rates [°/s])

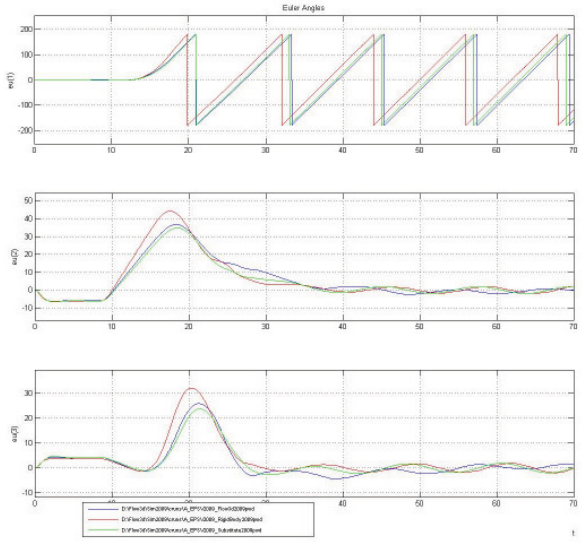

Fig. 9 Comparison of the simulation results (Euler Angles [°])

Fig. 10 and Fig. 11 show the torques acting around the rigid body Center of Gravity and the forces acting on the CoG of the rigid body. During powered flight the control torques are mainly acting around the transversal axes. In case of a coupled simulation the reaction torques caused by the sloshing mass are superimposed. The forces acting on the CoG are in this phase mainly thrust forces in longitudinal direction. In case of a coupled simulation the reaction forces caused by the sloshing mass, acting reverse to the thrust, reduces the residual force. During flight phases with RCS activations the impact of sloshing reduces with the activation of the nutation damping, yielding smoother sloshing behaviour.

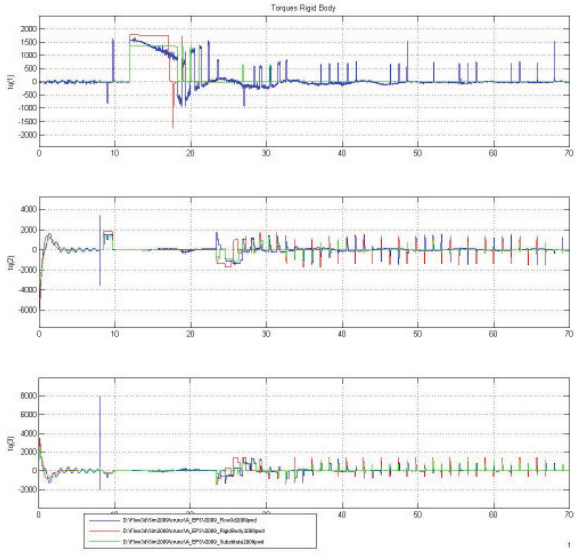

Fig. 10 Comparison of the simulation results (Torques acting on Rigid Body [Nm])

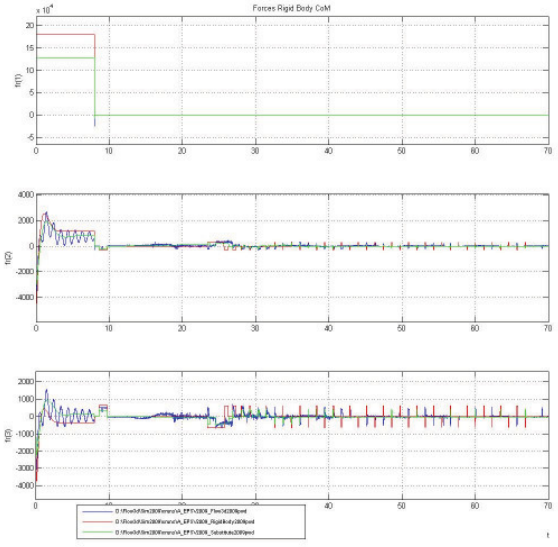

Fig. 11 Comparison of the simulation results (Forces Acting on Rigid Body CoG [N])

As expected the reaction forces and torques of the CFD coupled simulation are stronger pronounced than those of the simulation with a spring damper model. Of course the rigid body simulation shows no reaction forces and torques, see Fig. 12 and Fig. 13.

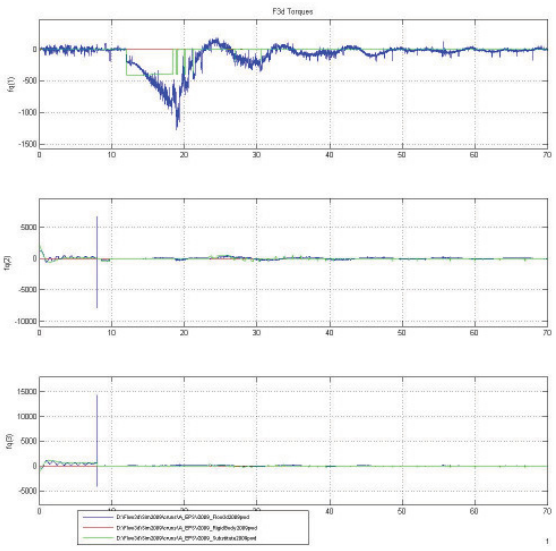

Fig. 12 Comparison of the simulation results (Reaction Torques [Nm])

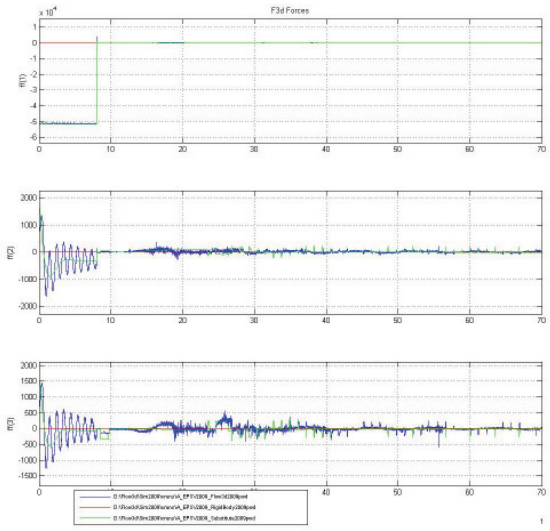

Fig. 13 Comparison of the simulation results (Reaction Forces [N])

3.2. Testing of the FLOW-3D / ESATAN coupling

For validation of the coupling between FLOW-3D and ESATAN, the analytical solution of a one-dimensional temperature field is used to check the coupling's functionality [5]. Considered is a medium, which is to one side infinite ($z \to \infty$). The temperature at infinity is ϑ_∞. At the medium's boundary ($z = 0$) the temperature suddenly changes from ϑ_∞ to ϑ_W. The asymptotical solution for the temperature field is:

(1) $$\frac{\vartheta - \vartheta_\infty}{\vartheta_W - \vartheta_\infty} = erf\left(\frac{z}{2 \cdot \sqrt{a \cdot t}}\right)$$

The thermal diffusivity a can be retrieved by:

(2) $$a = \frac{\lambda}{c \cdot \rho}$$

It is composed of the ratio of thermal conductivity λ to specific heat capacity c and density ρ. The temperature field is described by the Gaussian error function $erf(b)$:

(3) $$erf(b) = \frac{1}{\sqrt{\pi}} \cdot \int_0^b e^{-\xi^2} d\xi$$

Equation (1) is valid for Biot numbers which go towards infinity ($Bi \to \infty$). The Biot number Bi can be determined by:

(4) $$Bi = \frac{\alpha \cdot s}{\lambda}$$

with s as material thickness. The Biot number describes the relation of the inner thermal resistivity (s/λ) of the material to the outer heat-transmission resistance ($1/\alpha$). With the one-dimensional z-directed Fourier number

(5) $$Fo_z = \frac{a \cdot t}{z^2}$$

and

(6) $$\Theta = \frac{\vartheta - \vartheta_\infty}{\vartheta_W - \vartheta_\infty}$$

equation (1) can also written in a dimensionless form:

(7) $$\Theta = erf\left(\frac{1}{2 \cdot \sqrt{Fo_z}}\right)$$

The use of equation (1) is valid for infinite media, as mentioned above. A non-infinite medium can be considered infinite for small time spans. For longer time spans, a different approach is required. The condition for longer time spans is $Fo_z > 0.5$. If this condition is fulfilled, the following equation is valid instead of equation (1):

(8) $$\Theta = \frac{4}{\pi} \cos\left(\frac{\pi}{2} \frac{z}{s}\right) \cdot e^{-\frac{\pi^2}{4} \cdot Fo_z}$$

In order to prove the functionality of the coupling, at first a simple case is considered to check, whether values are exchanged correctly between FLOW-3D and ESATAN. For simplicity the ESATAN model is changed such that wall temperatures are kept constant. This is done by setting the node capacities to a high value, like for example to 10^{99}. A comparison of the temperature distribution between analytical approach and numerical simulation are displayed in Fig. 14 to Fig. 16. The temperatures are displayed for distinct time steps at t = 1000 s, 2000 s and 3000 s respectively. In each figure, the graph represents the analytic solution and the dots the solution retrieved from the numerical solution for the cells.

All three figures show, that there is consistency between the data retrieved from the numerical solution and the data calculated analytically. The temperature conductivity of LOX is comparably poor. This is why there is only a weak progress of the temperature against the distance from the tank wall within the first seconds. In order to show visible results, a time step size of 1000 s was chosen for the three diagrams. On comparing the three figures it can be seen, that the temperature field moves very slowly into the liquid. As the condition $Fo_z > 0.5$ is not fulfilled for none of the cells during the considered simulation time of 3000 s, no analytical calculations with equation (8) were conducted. [5]

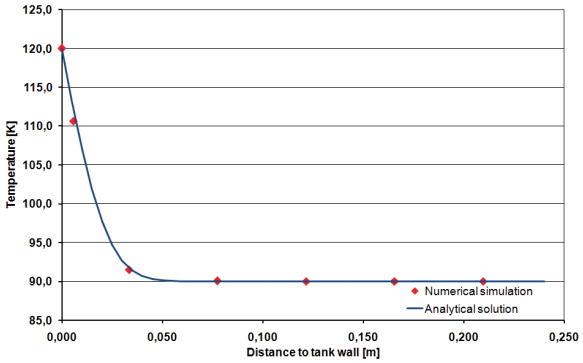

Fig. 14 Comparison of the analytical calculations by means of equation (1) with the numerical results of the simulation with the coupling for the temperature field within the fluid in a resting state and zero gravity at t = 1000 s

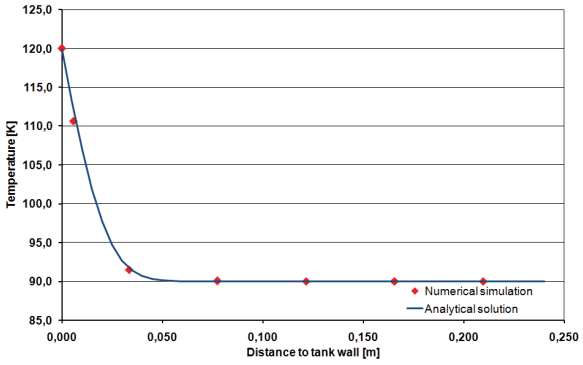

Fig. 15 Comparison of the analytical calculations by means of equation (1) with the numerical results of the simulation with the coupling for the temperature field within the fluid in a resting state and zero gravity at t = 2000 s

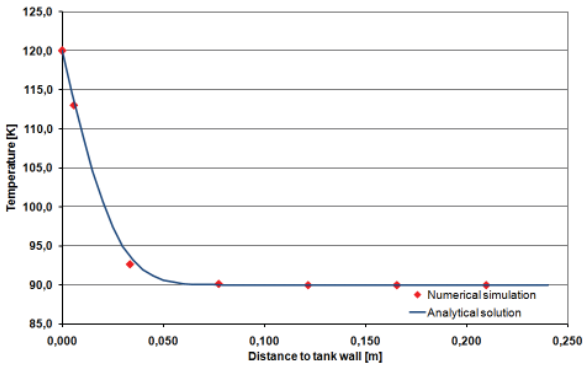

Fig. 16 Comparison of the analytical calculations by means of equation (1) with the numerical results of the simulation with the coupling for the temperature field within the fluid in a resting state and zero gravity at t = 2000 s

3.3. Verification of the FLOW-3D / ESATAN coupling with Ariane 5 ESC-A flight data

On February 12th 2005 the first flight of the Ariane 5 cryogenic upper stage ESC-A was successfully carried out. In the frame of a post-mission analysis the flight data were evaluated in detail in order to investigate the propellant and thermodynamic behaviour during the flight. First analyses concerning the post flight analysis were presented in [2]. In the present case the same data set is used to verify the coupling method between ESATAN and FLOW-3D in a realistic flight scenario.

The considered ballistic phase consists of a number of redirection manoeuvres and a spin-up phase of the stage to 10°/s for P/L release as shown in Fig. 17, t = 1900 seconds after lift-off. [2]

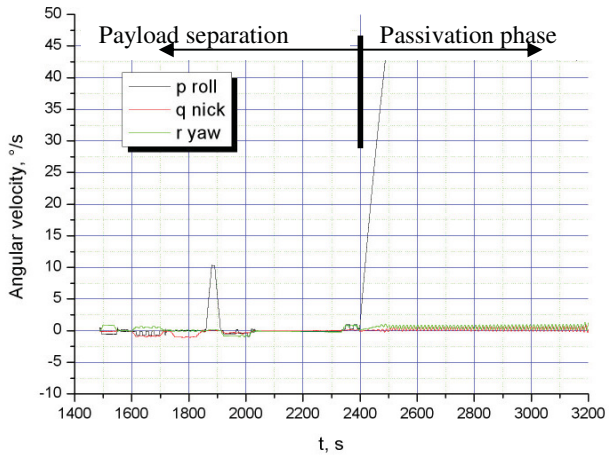

Fig. 17 Angular velocity profile during ballistic phase with payload release [2]

At t = 2400 seconds a spin-up to 45°/s occurs, followed by a passivation of the system at high spin rates. Several temperature sensors were implemented in and around the tank providing information concerning the propellant stratification. During the ballistic phase these transducers can be used as liquid markers in order to assess the liquid location in the tanks. The different sensors were

introduced into the FLOW-3D® model in order to enable a comparison with the flight data [2]. A view of the fluid behaviour for selected time steps is shown in the following pictures for the ESC-A LH2 tank. At $t = 0s$ the liquid is assumed to be settled at the tank bottom. This corresponds to $t = 1487s$ in Fig. 17.

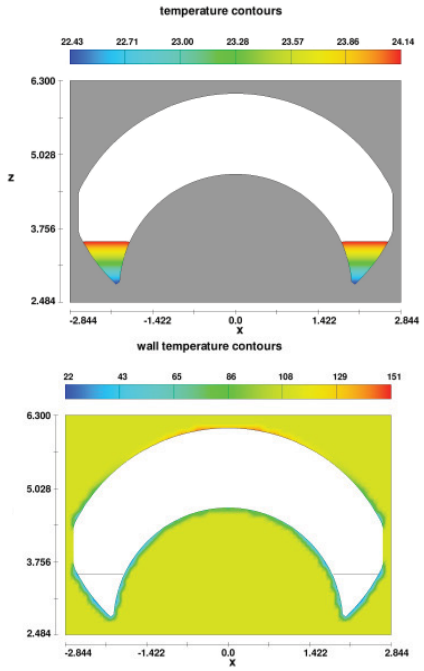

Fig. 18 Liquid and wall temperature distribution in the LH2 tank (here: initial condition at $t = 0s$)

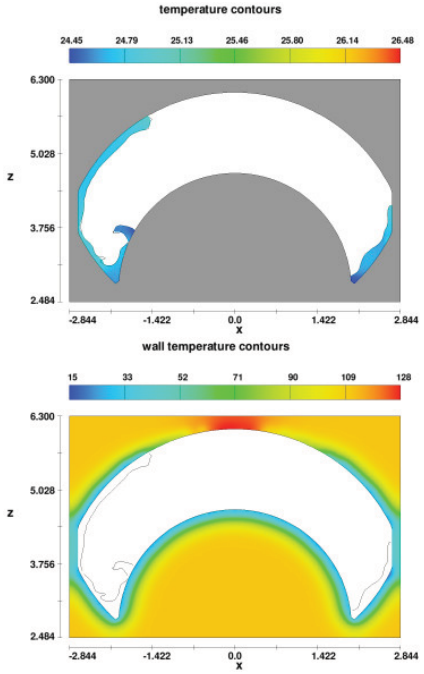

Fig. 19 Liquid and wall temperature distribution in the LH2 tank (here: initial condition at $t = 360s$)

Initially at $t = 0s$ a high temperature gradient exists between the lower part of the tank wall and the upper dome. The temperature gradient reduces when the cold liquid climbs the upper dome (see Fig. 19). A strong temperature drop is also observed at wetted surfaces.

For better quantitative comparison of the flight data a number of sensors data readings were compared to the analysis results. The locations of two considered temperature sensors are shown in the following graph.

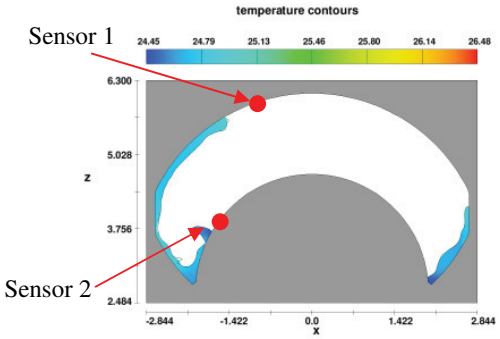

Fig. 20 Selected temperature sensors at the tank wall of the ESC-A LH2 tank

One chosen sensor is located near the top of the upper dome. The second sensor is located at the lower tank sphere.

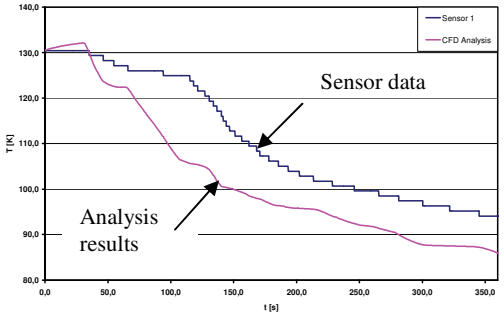

Fig. 21 Sensor 1 temperature history at the tank wall in the LH2 tank, comparing the sensor data with the analysis results. t=0 corresponds to a physical flight time of 1487 seconds

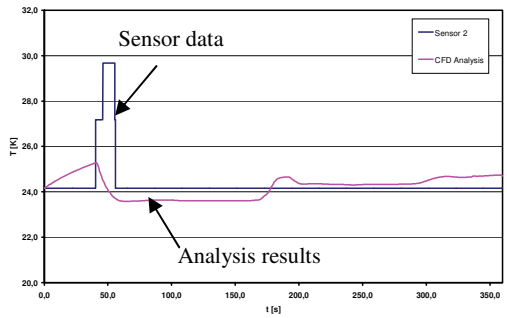

Fig. 22 Sensor 2 temperature history at the tank wall in the LH2 tank, comparing the sensor data with the analysis results. t=0 corresponds to a physical flight time of 1487 seconds

It can be seen that the results of the simulation by means of the thermal coupling shown the same tendency compared to the measured data, as far as changes in temperature are concerned. However, the simulated temperatures do not fully reach the measured ones, although starting from the same initial temperature. The differences in temperature are a consequence of the simplified modelling, in which the tank is considered as a closed system with no heat input from the outside of the system. Further, one-phase modelling of the fluid(s) within the tank was selected for the simulation and pressurization with Helium gas, which represents a major heat source, was fully neglected. For the future a more detailed modelling is aspired in order to conduct a second comparison. The comparison however shows that the new coupling method is able to tackle realistic flight scenarios. Considering more realistic boundary conditions, better matches between CFD and flight data are expected.

4. RESULTS

In order to demonstrate the capability of the tool, a realistic flight scenario was evaluated with respect to its sloshing behaviour during a ballistic flight phase. The angular rates and the applied thruster pulses are depicted in Fig. 23 and Fig. 24.

The mission scenario can be split into two main parts which is a slewing manoeuvre, occurring during the first 200 seconds. After a 200 seconds waiting phase, the stage is spun up to 1 °/s spin at t=400 s.

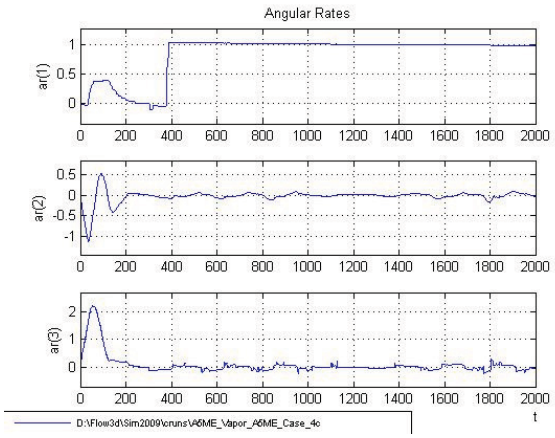

Fig. 23 Angular rates (ar(1): role rate; ar(2): nick rate; ar(3): yaw rate [°/s])

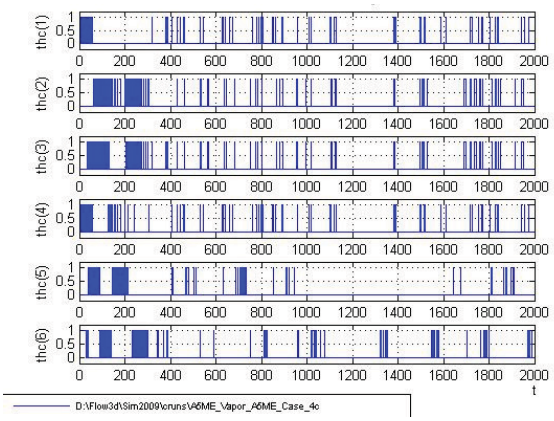

Fig. 24: Thruster commands for the different RCS thrusters

The different mission sequences will be discussed in more detail in the following.

4.1. Ballistic flight phase: 180° Slewing

Fig. 25 shows the motion of the stage during the slewing manoeuvre. Initially the liquid is considered to be settled as expected after a main thrust phase.

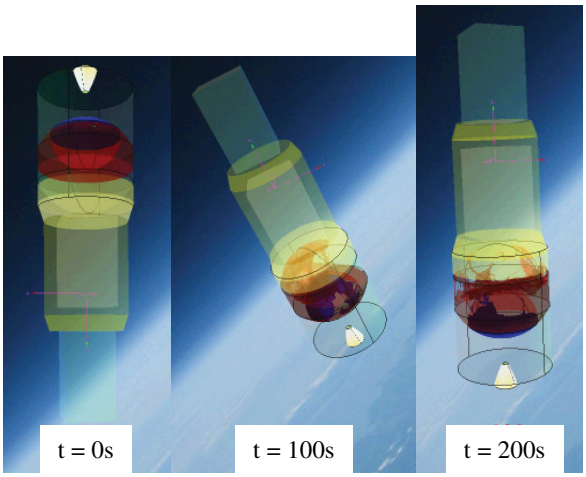

Fig. 25 Slewing manoeuvre: The stage is turned 180°.

The slewing manoeuvre leads to large sloshing motions which occur during acceleration at the beginning and de-acceleration after the maximum slewing rate of here 2°/s is reached. The switch from acceleration to de-acceleration leads to large sloshing motions.

The present configuration considers two payloads to be mounted on the stage. The centre of gravity is therefore above the tank such that the liquid anticipates to settle at the tank bottom.

4.2. Ballistic flight phase: 1 °/s spin

At t=400s the stage is spun up to 1 °/s. Under ideal, static conditions, the liquid would settle stable at the outer tank

walls. This is depicted in Fig. 26 for the Ariane 5 A5ME upper stage, here considering a fill level of 10%.

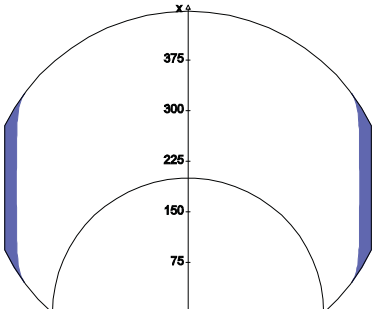

Fig. 26: Static propellant condition for a spin rate of 1°/s and 10% fill level, here concerning the Ariane 5 A5ME LH2 propellant tank

Under realistic conditions, considering thruster activations, the liquid will however not be settled at the tank wall. This can be seen when viewing the following pictures for t=400s (start of spin-up), and t=1000s as well as t=2000s (see Fig. 27).

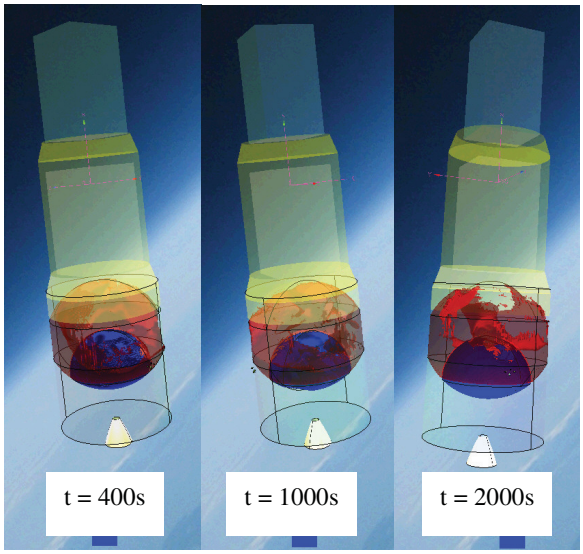

Fig. 27 Spin-up to 1°/s at 400s, keeping the spin rate constant

About all tank walls are wetted for both LH2 (liquid in red color) and LOX tank (liquid in blue color).

This shows that a sufficiently accurate prediction of the wetting conditions in the present case requires the consideration of the ballistic phase in a closed loop environment (RCS + rigid body motion + fluid mechanics in tanks).

The knowledge concerning wetting conditions at the tank walls is of importance in case of cryogenic tanks since evaporation and condensation effects occur, changing also the tank pressure.

5. SUMMARY AND CONCLUSION

Ballistic flight phases for cryogenic upper stages impose the need to analyze the sloshing behaviour in the propellant tanks, taking into account the RCS manoeuvres as well as the temperature evolution. A tool was therefore developed which enables a closed loop analysis of the stage behaviour, taking into account the stage controller as well as the fluid dynamics in the tanks. In addition a coupling of the propellant thermodynamics in the tanks, modelled with the CFD tool FLOW-3D [3], and the thermodynamics of the stage structure, modelled with the tool ESATAN [4], was introduced. First steps concerning a verification of the tool were conducted. It is anticipated to conclude these verification steps, providing an adequate means for modelling these coupled phenomena, occurring in a ballistic environment.

It is anticipated to use the developed tool for the layout of future upper stages. The tool may however also be used to analyze the fluid dynamic behaviour in non-space vehicles, e.g. air planes or tanker ships.

6. ACKNOWLEDGEMENT

The authors would like to thank the Deutsches Zentrum für Luft- und Raumfahrt (DLR) for their continuous support.

7. ABBREVIATIONS

GTO	Geostationary Transfer Orbit
ESC	Étage Supérieur Cryogenique
CFD	Computational Fluid Dynamics
FiPS	Final Phase Simulator
A5ME	Ariane 5 Midterm Evolution
RCS	Reaction Control System
CoG	Centre of Gravity
P/L	Payload

8. REFERENCES

[1] H. Klotz, R. Burkert, "Coupled Flow-3D Simulation for Analysis & Modelling of Dynamics of Upper Stages Containing Liquids", 5th International Conference on Launcher Technology, Madrid, Spain, 25th-27th November 2003

[2] P. Behruzi, M. Michaelis, and G. Khimeche, "Behaviour of the Cryogenic Propellant Tanks during the First Flight of the Ariane 5 ESC-A Upper Stage", AIAA 2006-5052, 42nd Joint Propulsion Conf. and Exhibit, Sacramento, USA, 2006

[3] URL: www.flow3d.com

[4] ITP ENGINES UK LTD., ESATAN-TMS Thermal Engineering Manual, Leicester, 2009

[5] Netzlaf, P., "Numerical Simulation of Fluid-Structure Interactions with Cryogenic Propellants of Rocket Stages", Diploma Thesis, Institut für Strömungsmechanik, Technische Universität Braunschweig, April 2011